“© 2022 IEEE. Personal use of this material is permitted. Permission from IEEE must be obtained for all other uses, in any current or future media, including reprinting/republishing this material for advertising or promotional purposes, creating new collective works, for resale or redistribution to servers or lists, or reuse of any copyrighted component of this work in other works.”

Frequency-Hopping Based Joint Automotive Radar-Communication Systems Using A Single Device

Zhitong Ni[1,2], J. Andrew Zhang[2], Kai Yang[1], and Renping Liu[2]
[1] Beijing Institute of Technology, School of Information and Electronics, China
[2] University of Technology Sydney, Global Big Data Technologies Centre (GBDTC), Australia
zhitong.ni@student.uts.edu.au; Andrew.Zhang@uts.edu.au; yangkai@bit.edu.cn; renping.liu@uts.edu.au.

***Abstract*—Dual-functional radar-communication (DFRC), integrating the two functions into one system and sharing one transmitted signal, shows its great potential in self-driving networks. In this paper, we develop a single-device based multi-input single-output (MISO) DFRC vehicular system. Modulations of un-slotted ALOHA frequency-hopping (UA-FH) and fast FH, commonly used in automotive radar, are adopted to transmit the DFRC waveforms and to address severe interferences caused by an interfering vehicle that serves as a communication transmitter. Due to the asynchrony between vehicles, the FH sequences of the interfering vehicle are chosen from a fixed codebook. All channel parameters are then extracted via FH decoding from radar backscattered channels and communication channels, respectively. To further increase the accuracy, we proceed to propose an iterative algorithm that divides the signals into short segments and jointly obtains all parameters with high resolution. Finally, simulation results are provided and validate the proposed DFRC vehicular system.**

***Index Terms*—Joint communication and radar sensing, dual-functional radar-communications, frequency-modulated continuous wave (FMCW) radar, frequency hopping**

I. Introduction

Transmitting an integrated waveform and sharing the spectrum together, dual-functional radar-communication (DFRC) is a promising technique that will be used in many applications. One main application is in vehicular networks and self-driving [1], [2], where signals used for communications between cars are also used for sensing the environment or vice versa. With sharing radar and communication functions, the DFRC devices can be smarter and faster than conventional electronic devices. Moreover, thanks to the fused functions and the shares of hardware resources, DFRC techniques can save hardware costs and reduce power consumption significantly with the deployment of a huge number of electronic devices in the future applications [3].

Automotive radar has been used in cars for a long time since 1949 [4]. Currently, the main techniques used in automotive radar include frequency-modulated continuous-wave (FMCW) radar and its variants [5]. The FMCW radar continuously transmits a set of chirp signals. By using a reference signal at the receiver side, the targets can be detected with high resolution due to the large bandwidth of the chirp signals. However, the existence of interferences caused by surrounding interfering vehicles is inevitable, and it leads to a severe rise for both missing alarm rate and false alarm rate [6], [7]. To address the interference issues, there exist some FMCW variants, including multiple frequency-shift-keying (MFSK) [8], varying the chirps' slop [4], un-slotted ALOHA frequency-hopping (UA-FH), and UA-FH phase coding (PC) [9].

Automotive radar only focuses on realizing the radar functions in cars. The DFRC based automotive systems have been studied in the literature [10], [11]. In [10], the authors employed phase-modulated continuous-wave (PMCW) for radar sensing and embedded the communication functions using differential phase-shift keying (DPSK). The authors used fast Fourier transform (FFT) and MUSIC methods for estimating the parameters of radar channels. In [11], the authors focused on vehicle-to-vehicle (V2V) joint communications and radar using 802.11ad standards. Their proposed sensing methods require a line-of-sight (LOS) path between source and recipient node, which is not always available when another vehicle overtakes the receiver and block the LOS path. It is noted that the above-mentioned papers have an assumption that each node has two separate devices that are in the front and the back of the node, respectively, where one device is a DFRC system that transmits the DFRC signals and receives the backscattered signals for sensing, and the other one serves as a communication receiver to realize the communication link. Their adopted DRFC system would require full-duplex technologies to realize a simultaneous transmission and receiving of signals, while the full-duplex is not quite mature at the current moment [12].

Inspired by the variants of FMCW radar, this paper develops a DFRC system for vehicular networks. To reduce the number of devices required, this paper uses only one set of DFRC devices, which can be fixed on the top of a node, to realize simultaneous backscattered radar sensing and V2V communications. We mainly consider two types of FMCW variants. One is based on UA-FH and the other one is fast FH. These two modulations can significantly reduce the interference caused by the interfering vehicle. Aiming to obtain the channel parameters, we propose a two-step sequential sensing method. The first step is based on FH decoding, where the parameters can be estimated with relatively low resolution. The second

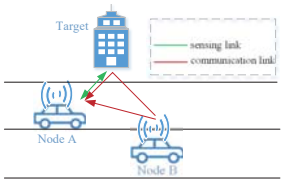

Fig. 1. Considered scenarios where a victim vehicle detects targets with suffering from the interference signals from an interfering vehicle.

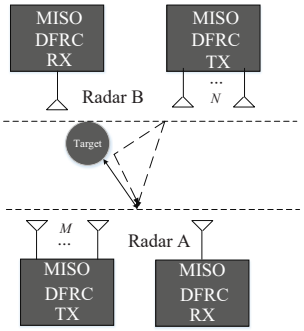

Fig. 2. Illustration of the MISO DFRC system architecture.

step is an iterative algorithm that uses the estimates from the first step as inputs and iteratively improves the accuracy of the estimates.

II. System and Channel Models

The main considered scenario of this paper is DFRC based automotive networks, as shown in Fig. 1, where multiple cars conduct radar sensing and communication simultaneously. The victim radar (Node A), equipped on the top of a vehicle, receives its backscattered signal for detecting targets and the strong interference signals from other vehicles (Node B). Conventionally, both the interfering radar and the victim radar adopt FMCW signals due to the high resolution. Our adopted system employs two variants of the FMCW signal, i.e., UA-FH and fast FH, such that the interference can be used to realize the communication functions. The UA-FH signal can be easily degraded into either chirp signals or fast FH signals, which is illustrated below (2). Hence, we integrate these two signals into one form that is equivalent to UA-FH. Both UA-FH and fast FH provide a good tradeoff for balancing between the communication (smaller bandwidth) and sensing (larger bandwidth) requirements and depress the interferences of the interfering radar greatly. Each node/radar uses a random and unique FH code.

It should be highlighted that each node has only one DFRC device to realize both functions and does not need a separate communication receiver, as shown in Fig. 2. Radar A (node A) transmits its sensing signals and receives both the backscattered signals and the interference signals from radar B (node B). The transmitters (TX) have M antenna elements and the receivers (RX) have one antenna element for each node/radar. The adopted FMCW modulation is based on UA-FH. Each radar transmits the sensing signals with initial frequencies randomly varying among different hops and antennas. Denote the carrier frequency of the FH radar as f_{L} and the total bandwidth as B. By dividing the frequency band evenly into K sub-bands, the kth initial frequency is given by $f_k = f_{\mathrm{L}} + \frac{k}{K}B$. The indices of hopping frequencies are selected from $\{0, \cdots, K-1\}$ arbitrarily for different hops. The FH signals of length H are periodically transmitted L times in a coherent processing interval (CPI). The hopping frequency at the hth hop and the mth antenna is denoted as $f_{h,m}$ and should satisfy

$$f_{h,m} \neq f_{h,m'}, \forall h \in \{0, \cdots, H-1\}, \forall m \neq m'. \quad (1)$$

In UA-FH, the DFRC radar transmits chirp signals in each hop with the frequency linearly increased in a bandwidth of B/K. The transmitted sensing signal of node A at the mth antenna of the hth hop is given by

$$x_{h,m}(t) = s_m D_h e^{j2\pi(f_{h,m}+\frac{tB}{TK})t}\mathrm{rect}_T(t), \quad (2)$$

where T is the duration of one hop, D_h is the pilot/data symbol, and s_m is the mth element of the transmitted waveform. During channel estimation period, D_h is known pilot signals. In the data transmission period, D_h/D_{h-1} denotes a data symbol in a limited set of constellations. We would like to use analog arrays for the beamforming vector. Hence, s_m should satisfy $|s_m| = 1$. It is noted that the UA-FH signals in (2) can be degraded into chirp signals and fast FH signals. When removing the term of $\frac{tB}{TK}$, the signals become fast FH signals. When removing the term of $f_{h,m}$ and making $K = 1$, the signals become chirp signals.

Node A receives its own sensing signal. Meanwhile, in the DFRC systems, it also serves as a communication receiver. Hence, node B's interference signals can be used to realize communications between A and B. It is the same for node B, which simultaneously receives its own backscattered sensing signals and node A's interfering signals for communication purposes. For notational simplicity, we view this system from the perspective of node A and regard node B as a node of communication transmitter. At node B's side, the same transmit procedure is employed with the equipment of M transmit antennas. The transmitted DFRC signal of node B is

$$x'_{h,m}(t) = s'_m D'_h e^{j2\pi(f'_{h,m}+\frac{tB}{TK})t}\mathrm{rect}_T(t), \quad (3)$$

where $x'_{h,m}(t)$ is the transmitted signal at the mth antenna of the hth hop of node B, s'_m is the mth element of B's waveform, such that $|s'_m| = 1$, D'_h is the pilot/data symbol, and the hopping frequencies are denoted as $f'_{h,m}$.

We assume that there is one target. When there exist multiple targets, a similar scheme can be derived. The node A's received signal can be given by

$$y(t) = \alpha \sum_{h=0}^{H-1} \mathbf{a}^H(\theta)\mathbf{x}_h(t - \tau + \nu t - hT)$$

$$+\alpha' \sum_{h=0}^{H-1} \mathbf{a}^H(\theta')\mathbf{x'}_h(t-\tau'+\nu' t-hT)$$
$$+\alpha_0 \sum_{h=0}^{H-1} \mathbf{a}^H(\theta_0)\mathbf{x'}_h(t-\tau_0+\nu_0 t-hT)+n(t), \quad (4)$$

where $\mathbf{x}_h(t) = [x_{h,1}(t), \cdots, x_{h,M}(t)]^T$, $\mathbf{x}'_h(t) = [x'_{h,1}(t), \cdots, x'_{h,M}(t)]^T$, $\mathbf{a}(\cdot)$ denotes an array steering vector, and $n(t)$ is an additive white Gaussian noise (AWGN); θ and θ' denote the angles-of-departure (AoDs) of the target with respect to (w.r.t.) node A's transmitter (TX A) and node B's transmitter (TX B), respectively, and θ_0 denotes the LOS AoD between node A's receiver (RX A) and TX B; τ and τ' denote the propagation delays via the paths of TX A-target-RX A and TX B-target-RX A, respectively, and τ_0 denotes the LOS delay between RX A and TX B; ν and ν' denote the Doppler shifts via the paths of TX A-target-RX A and TX B-target-RX A, respectively, and ν_0 denotes the LOS Doppler shift between A and B; α, α', and α_0 denote the path loss w.r.t. the corresponding paths, respectively.

In this paper, we propose a two-step parameter estimation scheme for all unknown parameters in (4). The first step will be illustrated in section III and the second step will be illustrated in section IV.

III. Parameter Estimation for Individual Purposes

A. Parameter Estimation for Radar Sensing

In this subsection, we focus on node A's sensing functions through estimating the parameters for radar purposes, i.e., α, θ, τ, and ν.

At the A's receiver, the received signal is down-converted to the baseband by multiplying a single-frequency signal with the frequency of f_{L}. The baseband signals for node A's receiver can be given by

$$\begin{aligned} & r(t) \\ =& y(t)e^{-j2\pi f_{\mathrm{L}} t} \\ =& y(t)\sum_{h=0}^{H-1} e^{-j2\pi f_{\mathrm{L}}(t-\tau-hT)}\mathrm{rect}_T(t-\tau-hT)e^{j2\pi f_{\mathrm{L}}(\tau+hT)}. \end{aligned} \quad (5)$$

To avoid the influence of the carrier frequency, $e^{j2\pi f_{\mathrm{L}}(hT)}$ should equal 1 and the term of $e^{j2\pi f_{\mathrm{L}}\tau}$ is a fixed value that can be absorbed into the complex path gains. For each antenna m, we utilize the low correlation of different FH sequences and obtain the decoded signal via multiplying a reference signal. The decoded signal for node A is

$$r_m(t) = r(t) * \sum_{h=0}^{H-1} e^{j2\pi(f_{h,m}-f_{\mathrm{L}}+\frac{tB}{TK})t}\mathrm{rect}_T(t-hT), \quad (6)$$

where $*$ means convolution between two signals.

We can estimate the parameters for radar purposes as follows. The delay term can be easily obtained by finding the peak in the decoded signals due to the low correlation between different FH sequences. In a period of H hops, the Doppler term varies slightly and can be neglected. We use a CPI with L same transmit signals to obtain the phase variance caused by the Doppler term. The AoD term can be estimated using the phase variance of the peaks in the spatial domain. Hence, the estimates of AoDs are obtained after the delay is obtained, whereas the delay term can be estimated individually. As for the path gain, it is obtained after all delays, AODs, and Doppler shifts are obtained, which is shown in (7).

In the estimation scheme above, the signals from node B is seen as interference. When M is close to K or when the LOS path between node A and node B exists, the interference can dramatically degrade the estimation accuracy for radar sensing purposes.

B. Parameter Estimation for Communication

In this subsection, we will focus on estimating parameters for communication purposes. It is noted that the second and the third term in (4) consist of the communication channel between node A and node B. Hence, it is equivalent to a communication channel with two paths, where one path is the LOS path and the other one is a non-LOS (NLOS) path. Since node A has no prior knowledge about node B, it cannot execute the same estimation scheme as in the former subsection. The parameter estimation for communication purposes should tackle two technical problems. 1) How to obtain the FH sequence that is used by each antenna of node B? 2) How to match the parameters for each path of node B?

It is noted that the power of the LOS path of node B is much larger than that of other paths. Hence, in each hop, the frequency band with dominating power is denoted as $\mathcal{S}_h^B = \{\mathcal{B}_{h,1}, \cdots, \mathcal{B}_{h,Q}\}$, where Q, $M \le Q \le 2M$, denotes the number of dominating frequency bands, and $\mathcal{B}$ denotes a frequency band with the bandwidth of B/K and the initial frequency chosen from $\{f_k\}$. By combining H sets of $\mathcal{S}_h^B$, we form a sequenced cell as $\mathcal{C} = [\mathcal{S}_0^B, \cdots, \mathcal{S}_{H-1}^B]$. The hopping frequencies in each hop are most likely to be selected from $\mathcal{S}_h^B$. Using $\mathcal{C}$, the FH sequences of node B are ready to be obtained as long as the codebook has a limited size. This can be realized as follows.

Denote one codeword for the FH sequence as $\mathbf{w}_c, c \le C$, where $\mathbf{w}_c$ is an $H \times 1$ vector with each entry chosen from $\{f_k\}$ and C is the size of the codebook. If each entry of $\mathbf{w}_c$ can be found in each entry of $\mathcal{C}$, the codeword becomes a candidate codeword. With a given $\mathbf{w}_c$, the second codeword must meet the requirement of (1). Hence, the number of valid codewords is reduced. The second codeword is denoted as $\mathbf{w}'_c$ and the number of valid codewords is $C' \le C$. If each entry of the second codeword can also be found in each entry of $\mathcal{C}$. These two codewords consist of a candidate group, i.e., $\{\mathbf{w}'_c, \mathbf{w}_c\}$. Iteratively, we can obtain the third, the fourth, until the Mth codeword. In each iteration, the number of valid codewords is smaller than that of the former iterations because the new codeword needs to satisfy one more requirement. As long as the codebook has a limited size, we can obtain these M codewords almost for sure. In addition, if there are not M

candidate codewords that can both meet the requirement of (1) and be found in each entry of $\mathcal{C}$, we can use some modern techniques, such as machine learning, to find M codewords that are the closest to the obtained cell.

We note that the frequencies of each hop of node B are not matched with each antenna. This problem does not influence the estimation of delays and Doppler shifts since the delays and Doppler shifts are estimated in the time domain. Hence, both delays and Doppler shifts can be estimated using the same method in the former section without knowing the spatial order of codewords. The estimates of AoDs, however, have to obtain the spatial order of codewords. To tackle this problem, a simple way is to keep reducing the codebook size, such that M codewords form a group of sequenced codewords. This could make the codebook design be troublesome. We tend to use a fixed spatial order for all cars in the first H' hops, where $H' \ll H$.

After the FH sequence is known, we can use the same method in the former section to estimate the AoDs. Now, only the path gains are not obtained. The estimation of paths gains plays an important role in obtaining the data symbol during the data transmitting period. The estimation of path gains needs to be completed after the pair matching. As we mentioned in the first paragraph of this subsection, another issue to be addressed is that the estimated parameters need to be pair-matched since node B has two paths. Hence, after obtaining six parameters, including delays, Doppler shifts, and AoDs, these parameters need to match with the two paths respectively. We can estimate the AoDs and the Doppler shifts after the delay term. Decoding the FH sequences can generate two peaks representing two delay terms. All antennas have the same peaks. We use the phase variance on one of the peaks to estimate AoDs or Doppler shifts. Then, all parameters except path gains are estimated and pair-matched. It should be noted that the path gains of node B cannot be separated from $s'_m D'_h$, since $s'_m D'_h$ is also unknown. Hence, we can only obtain $\alpha' s'_m D'_h$ as a whole, which is the same for $\alpha_0 s'_m D'_h$. Using the LS method, we obtain the path gains at the hth hop and the mth antenna as

$$\begin{aligned}&\left[\hat{\alpha}, \hat{\alpha}_1 D_{h'} \mathbf{s}^T, \hat{\alpha}_0 D_{h''} \mathbf{s}^T\right]^T = \\ &\left[\begin{array}{c} \mathbf{a}^*(\hat{\theta}) \otimes \mathbf{x}_h(\mathbf{t}'_h - \hat{\tau} + \hat{\nu}\mathbf{t}'_h - hT) \\ \mathbf{a}^*(\hat{\theta}_1) \otimes \tilde{\mathbf{x}}_{h'}(\mathbf{t}'_h - \hat{\tau}_1 + \hat{\nu}_1 \mathbf{t}'_h - h'T) \\ \mathbf{a}^*(\hat{\theta}_0) \otimes \tilde{\mathbf{x}}_{h''}(\mathbf{t}'_h - \hat{\tau}_0 + \hat{\nu}_0 \mathbf{t}'_h - h''T) \end{array}\right]^{-1} r(\mathbf{t}_h) e^{j2\pi f_{\mathrm{L}} \mathbf{t}_h},\end{aligned} \tag{7}$$

where $\tilde{\mathbf{s}} = [s'_1, \cdots, s'_M]^T$, $\mathbf{t}'_h$ denotes a $(2M+1) \times 1$ discrete time vector in the period of $[hT, (h+1)T)$. With a given h, h' and h'' can be obtained accordingly, such that $\mathbf{x}_{h'}(\mathbf{t}'_h - \hat{\tau}_1 + \hat{\nu}_1 \mathbf{t}'_h - h'T)$ and $\mathbf{x}_{h''}(\mathbf{t} - \hat{\tau}_0 + \hat{\nu}_0 \mathbf{t}'_h - h''T)$ are not zeros.

IV. Parameter Estimation for Joint Radar and Communication Purposes

In the former section, all parameters can be estimated. In this section, we aim to enhance the estimation accuracy for both node A (radar sensing purposes) and node B (communication purposes). We propose an iterative algorithm that takes advantage of short-time Fourier transform (STFT) of signals. Before iterations, we need to obtain rough estimates for all parameters obtained from the former section. The estimates are divided into three groups, i.e., $(\hat{\alpha}, \hat{\theta}, \hat{\tau}, \hat{\nu})$, $(\hat{\alpha}', \hat{\theta}', \hat{\tau}', \hat{\nu}')$, and $(\hat{\alpha}_0, \hat{\theta}_0, \hat{\tau}_0, \hat{\nu}_0)$.

The antennas form a unique FH sequence of length M in each hop. We select a short-time segment, where the length of segment is T_S and the offset of the segment is ξ, and analyze its components in the frequency domain. The gth segment of node A is obtained as

$$r_g^A(t) = (r(t) - \hat{r}_{B_0}(t) - \hat{r}_{B'}(t)) \operatorname{rect}_{T_S}(t - \xi - gT_S), \tag{8}$$

where $\hat{r}_{B_0}(t)$ denotes the estimated signal for the LOS path of node B from former iteration, and $\hat{r}_{B'}(t)$ denotes the estimated signal for the NLOS path of node B. Likewise, we can obtain each segment for each path of node B as

$$r_g^{B'}(t) = (r(t) - \hat{r}_A(t) - \hat{r}_{B_0}(t)) \operatorname{rect}_{T_S}(t - \xi - gT_S), \tag{9}$$

and

$$r_g^{B_0}(t) = (r(t) - \hat{r}_A(t) - \hat{r}_{B'}(t)) \operatorname{rect}_{T_S}(t - \xi - gT_S), \tag{10}$$

where $\hat{r}_A(t)$ denotes the estimated signal of node A. We conduct the FFT for the samples of $r_g^A(t)$, $r_g^{B'}(t)$, and $r_g^{B_0}(t)$. These frequency-domain signals are denoted as $R_g^A[k]$, $R_g^{B'}[k]$, and $R_g^{B_0}[k]$, respectively.

On the other hand, we can directly construct $\hat{r}_g^A(t)$, $\hat{r}_g^{B'}(t)$, and $\hat{r}_g^{B_0}(t)$. Due to the page limits, we only give the formulation of $\hat{r}_g^A(t)$ as

$$\begin{aligned}&\hat{r}_g^A(t) \\ =&\hat{\alpha} \mathbf{a}^H(\hat{\theta}) \sum_{h=0}^{H-1} \mathbf{x}_h(t - \hat{\tau} + \hat{\nu}t - hT) e^{-j2\pi f_{\mathrm{L}} t} \\ &\cdot \operatorname{rect}_{T_S}(t - \xi - gT_S) \\ =&\hat{\alpha} \sum_{m=1}^{M} e^{j\pi(m-1)\sin(\hat{\theta})} \sum_{h=0}^{H-1} x_{h,m}(t - \hat{\tau} + \hat{\nu}t - hT) e^{-j2\pi f_{\mathrm{L}} t} \\ &\cdot \operatorname{rect}_{T_S}(t - \xi - gT_S) \\ =&\hat{\alpha} \sum_{m=1}^{M} \sum_{h=0}^{H-1} s_m D_h e^{j2\pi \left(k_{h,m} + (t - \hat{\tau} + \hat{\nu}t - hT)\frac{B}{TK}\right)(t - \hat{\tau} + \hat{\nu}t - hT)} \\ &\cdot e^{j\pi(m-1)\sin(\hat{\theta})} \operatorname{rect}_T(t - \hat{\tau} - hT) \cdot \operatorname{rect}_{T_S}(t - \xi - gT_S) \\ \approx&\hat{\alpha} \sum_{m=1}^{M} \sum_{h=0}^{H-1} s_m D_h e^{j2\pi \left(k_{h,m} + (t - \hat{\tau} - hT)\frac{B}{TK}\right)(t - \hat{\tau} - hT)} e^{j2\pi \hat{\nu} \frac{2B}{TK} t^2} \\ &\cdot e^{j\pi(m-1)\sin(\hat{\theta})} \operatorname{rect}_T(t - \hat{\tau} - hT) \cdot \operatorname{rect}_{T_S}(t - \xi - gT_S),\end{aligned} \tag{11}$$

where $k_{h,m} = f_{h,m} - f_{\mathrm{L}}$ is a discrete hopping frequency. In the same way, we can obtain $\hat{r}_g^{B'}(t)$, $\hat{r}_g^{B_0}(t)$. Note that $\hat{r}_A(t)$ can be generated by $\hat{r}_g^A(t)$ with arbitrary ξ and T_S. When $\xi = 0$ and $T_S = T$, $\hat{r}_A(t)$ can be obtained as $\sum_{g=1}^{H} \hat{r}_g^A(t)$. It is the same for the cases of $\hat{r}_{B'}(t)$ and $\hat{r}_{B_0}(t)$. We conduct

the FFT for the samples of $\hat{r}_g^A(t)$, $\hat{r}_g^{B'}(t)$, and $\hat{r}_g^{B_0}(t)$. These frequency-domain signals are denoted as $\hat{R}_g^A[k]$, $\hat{R}_g^{B'}[k]$, and $\hat{R}_g^{B_0}[k]$, respectively.

Ideally, $r_g^A(t)$ should be the same with $\hat{r}_g^A(t)$. Due to the imperfect estimation, both $r_g^A(t)$ and $\hat{r}_g^A(t)$ are distorted. The distortion of $r_g^A(t)$ is caused by the estimation error of $\hat{r}_{B_0}(t) + \hat{r}_{B'}(t)$. The distortion of $\hat{r}_g^A(t)$ is resulted from the estimation error of $(\hat{\alpha}, \hat{\theta}, \hat{\tau}, \hat{\nu})$. Directly counting the error between $r_g^A(t)$ and $\hat{r}_g^A(t)$ is invalid and cannot converge. Instead, we compute the energy in the mainly occupied frequency bands of $\hat{r}_A(t)$, which is operated as follows. The desired energy is given by

$$E(\hat{\tau}, \hat{\theta}, \hat{\alpha}, \hat{\nu}) = \sum_k \left| R_g^A[k] \hat{R}_g^A[k] \right|^2 \delta_k, \tag{12}$$

where δ_k equals 1 or 0 and depends on occupied frequency bands of the ideal signal. For fast FH, δ_k is 1 when the frequency is $\{f_{h,m}\}_{m=1}^M$. The energy is the highest when the parameters, $(\hat{\alpha}, \hat{\theta}, \hat{\tau}, \hat{\nu})$, are the most accurate. When the parameters are close to its practical value, the function can be seen as a convex function and can converge to its optimal value.

Likewise, we can also increase the accuracy of $(\hat{\alpha}', \hat{\theta}', \hat{\tau}', \hat{\nu}')$ and $(\hat{\alpha}_0, \hat{\theta}_0, \hat{\tau}_0, \hat{\nu}_0)$. We can fix the two groups of estimates and improve the accuracy of a third group first. For instance, we fix $(\hat{\alpha}', \hat{\theta}', \hat{\tau}', \hat{\nu}')$ and $(\hat{\alpha}_0, \hat{\theta}_0, \hat{\tau}_0, \hat{\nu}_0)$. Then, by substituting the improved $(\hat{\alpha}, \hat{\theta}, \hat{\tau}, \hat{\nu})$ into (9) and (10), respectively, we improve the accuracy of the unfixed group. These three groups of parameters can be improved in a cycle until the estimates remain unchanged. In general, $(\hat{\alpha}_0, \hat{\theta}_0, \hat{\tau}_0, \hat{\nu}_0)$ has a great accuracy before the iterations due to the dominating power of the LOS path.

V. Information Embedding and Data Transmission Scheme

Now, we embed the information and start the data transmission between node A and node B. Due to the asynchronism between node A and B, the transmitted waveform, $s'_m D'_h$ is unavailable at node A's receiver. During the communication channel estimation period, node B sends a random waveform without embedding information. After the FH sequences and all parameters of node B are obtained, we would like to carry information on D'_h to realize a data stream transmitted from node B to node A. However, there occur two problems that have to be addressed. One is that the communication channel is known by node A instead of node B. The other problem is when to embed data symbols for node B? In this section, we will solve these two problems and realize the communication purposes.

After node A obtains all parameters, node A begins to vary the symbol of D_h, such that D_h/D_{h-1} is a data symbol that varies in a limited constellation set. The first $H-1$ data symbols need to be different from the pilot sequence, thus the radar B can observe the variance of node A by obtaining $\hat{\beta}'_{h,m} = \beta' s_m D_h$ and $\hat{\beta}''_{h,m} = \beta_0 s_m D_h$, where β' is the path gain via TX A-target-RX B and $\beta_0 \approx \alpha_0$ is the LOS path gain from node A to node B. The data symbol of node A can be retrieved as

$$\frac{D_h}{D_{h-1}} = \frac{\hat{\beta}''_{h,m}}{\hat{\beta}''_{h-1,m}} = \frac{\hat{\beta}'_{h,m}}{\hat{\beta}'_{h-1,m}}. \tag{13}$$

It should be noted that, in the channel estimation period, $\frac{D_h}{D_{h-1}}$ is known values. At the beginning of the data transmission period, as long as $\frac{D_h}{D_{h-1}}$ is not the same as the pilot sequence, node B can be aware of the changes of node A's transmitted signal structure. Then, $\frac{D_h}{D_{h-1}}$ can be used to send node A's obtained estimates to node B. After node B obtains its channel knowledge, it designs its waveform, s'_m, to improve the communication performance and starts to realize the communication functions. The detailed protocol is beyond the scope of this paper. In the same way, node A can obtain its communication channel knowledge from node B.

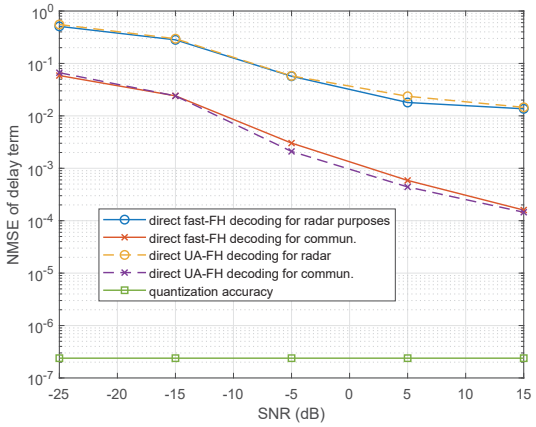

Fig. 3. NMSE of delay estimates versus SNR via using different modulated signals for both radar/node A and radar/node B, where SNR is the ratio of the transmit power to noise variance and the transmit power is fixed as 50 W.

VI. Simulation Results

In this section, we conduct simulations to verify the parameter estimation scheme in section III and IV. The system model can be referred to section II. Node A is equipped with $M = 12$ antennas, which is the same for node B. The adopted baseband bandwidth is 100 MHz that is divided into $K = 32$ sub-bands. The carrier frequency is 35 GHz. In one CPI, each transmitter transmits $L = 100$ cycles with $H = 64$ hops. Each hop has a duration of $T = 320$ ns. The BF weights are a constant-modulus value with random phase shift. The delay term varies uniformly from 0 to 1.6 us. The Doppler shift term equals v/c, where v is the radius speed of cars that ranges from -108 kph to 108 kph, and c is the speed of light. Hence, the Doppler term varies from -10^{-7} to 10^{-7}. The AoD term varies uniformly from $-\pi$ to π.

Fig. 3 presents the normalized mean-squared-error (NMSE) via using fast-FH and UA-FH signals, where the UA-FH signals are shown in (2). By removing the term of $\frac{tB}{TK}$,

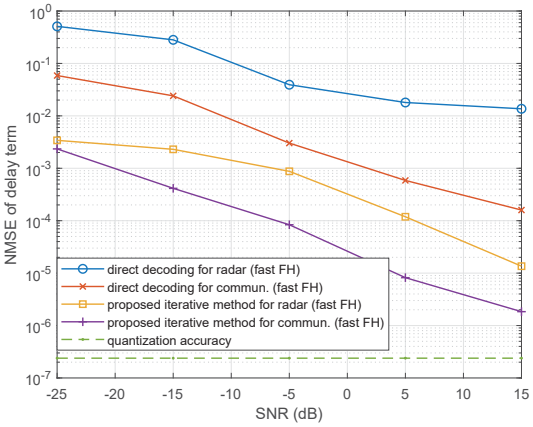

Fig. 4. Performance of delay estimates by using the proposed iterative algorithm on fast FH signals.

the signals become the fast FH signals. Node A receives its own backscattered signals for radar purposes and receives the signals of node B for communication purposes. The estimates of delays are obtained via direct decoding as described in section III. Note there is a LOS path between node A and node B. The path gain of the LOS path is 10 dB higher than the NLOS path. From the figure, it can be seen that, the NMSE of node A's delay term is significantly higher than that of node B's delay, which means the accuracy of the communication channel (node B) is significantly higher than that of radar channel (node A), even though node A has no prior knowledge about node B. This is mainly because node B contributes a LOS-path signal in node A's received signals. The quantization accuracy is written as $\frac{1}{H^2 N_{\text{spl}}^2}$ with $N_{\text{spl}} = 32$ being the number of samples per hop. Compared between fast-FH and UA-FH modulation, we see that the UA-FH signals and fast FH signals perform nearly the same. This is because the FH sequence is long enough to extract the FH sequence. It should be noted that the performance can be improved by using a larger K or H, which would cause the efficiency to decrease.

To improve the performance of node A using the same setup, we adopt the fast-FH signals only and employ the proposed iterative algorithm with $T_S = T$ and ξ being the estimated delay term. Fig. 4 shows the NMSE improvement for node A (radar purposes) and node B (communication purposes) under the same system setup as in Fig. 3. We fix the path gain terms and neglect the Doppler terms. The improvement of the proposed method is significant. We can see that both node A's channel and node B's channel reach lower NMSEs compared with their counterparts of direct decoding. The NMSE of radar is reduced from 10^{-2} to 10^{-5} at the SNR of 15 dB. The NMSE of radar is still higher than that of the communication channel, but it performs much better compared with the NMSE before iterations. It is also observed that the NMSEs after iterations perform nearly the same for communication and radar channels at a quite low. The results indicate that the proposed algorithm can overcome the severe interference of node B and improve the estimation accuracy of node A greatly.

VII. Conclusion

This paper proposed a joint radar and communication parameter estimation scheme for auto-vehicular networks. The estimates are first obtained by direct decoding via using the low correlation of FH sequences and then improved by using the proposed iterative algorithm that maximizes the desired energy. The results show that the fast FH modulations perform nearly the same as the UA-FH modulations. Combining with the proposed iterative algorithm, fast-FH is good enough to obtain high-resolution estimates. The proposed method also sheds light on how to retrieve a low-power signal under strong interference. Moreover, this paper only uses one set of devices to realize the DFRC system. The single device estimates the joint radar and communication channel and transmits data symbols between cars.

References

[1] R. C. Daniels, E. R. Yeh, and R. W. Heath, "Forward collision vehicular radar with IEEE 802.11: Feasibility demonstration through measurements," *IEEE Trans. Veh. Technol.*, vol. 67, no. 2, pp. 1404–1416, Feb. 2018.

[2] S. H. Dokhanchi, M. R. B. Shankar, Y. A. Nijsure, T. Stifter, S. Sedighi, and B. Ottersten, "Joint automotive radar-communications waveform design," in *2017 IEEE 28th Annual International Symposium on Personal, Indoor, and Mobile Radio Communications (PIMRC)*, Oct. 2017, pp. 1–7.

[3] F. Liu, C. Masouros, A. P. Petropulu, H. Griffiths, and L. Hanzo, "Joint radar and communication design: Applications, state-of-the-art, and the road ahead," *IEEE Trans. Commun.*, vol. 68, no. 6, pp. 3834–3862, Jun. 2020.

[4] C. Aydogdu, M. F. Keskin, G. K. Carvajal, O. Eriksson, H. Hellsten, H. Herbertsson, E. Nilsson, M. Rydstrom, K. Vanas, and H. Wymeersch, "Radar interference mitigation for automated driving: Exploring proactive strategies," *IEEE Signal Process. Mag.*, vol. 37, no. 4, pp. 72–84, 2020.

[5] S. M. Patole, M. Torlak, D. Wang, and M. Ali, "Automotive radars: A review of signal processing techniques," *IEEE Signal Process. Mag.*, vol. 34, no. 2, pp. 22–35, 2017.

[6] Z. Yang and A. Mani, "Interference mitigation for AWR/IWR devices," *Texas Instruments Inc., leden*, 2020.

[7] G. M. Brooker, "Mutual interference of millimeter-wave radar systems," *IEEE Trans. Electromagn. Compat.*, vol. 49, no. 1, pp. 170–181, 2007.

[8] H. Rohling, M. Kronauge, F. Gini, A. De Maio, and L. Patton, "Continuous waveforms for automotive radar systems," in *Waveform design and diversity for advanced radar systems*. IET, 2012, vol. 22, pp. 173–205.

[9] S. Jin and S. Roy, "FMCW radar network: Multiple access and interference mitigation," *IEEE J. Sel. Topics Signal Process.*, vol. 15, no. 4, pp. 968–979, 2021.

[10] S. H. Dokhanchi, M. R. B. Shankar, Y. A. Nijsure, T. Stifter, S. Sedighi, and B. Ottersten, "Joint automotive radar-communications waveform design," in *2017 IEEE 28th Annual International Symposium on Personal, Indoor, and Mobile Radio Communications (PIMRC)*, 2017, pp. 1–7.

[11] P. Kumari, J. Choi, N. González-Prelcic, and R. W. Heath, "IEEE 802.11ad-based radar: An approach to joint vehicular communication-radar system," *IEEE Trans. Veh. Technol.*, vol. 67, no. 4, pp. 3012–3027, Apr. 2018.

[12] Z. Zhang, X. Chai, K. Long, A. V. Vasilakos, and L. Hanzo, "Full duplex techniques for 5G networks: self-interference cancellation, protocol design, and relay selection," *IEEE Commun. Mag.*, vol. 53, no. 5, pp. 128–137, May 2015.